Pyridine Bridging Diphenylamine-Carbazole with Linking Topology as Rational Hole Transporter for Perovskite Solar Cells Fabrication

Peng Huang [a#], Manju [c#], Samrana Kazim [a,b], Gangala Sivakumar [c], Manuel Salado [a], Rajneesh Misra [c*], and Shahzada Ahmad [a,b*]

[a] BCMaterials, Basque Center for Materials, Applications and Nanostructures, Martina Casiano, UPV/EHU Science Park, 48940 Leioa, Spain

Tel: +34 946128811 E-mail: shahzada.ahmad@bcmaterials.net;

[b] IKERBASQUE, Basque Foundation for Science, Bilbao, 48013, Spain

[c] Department of Chemistry, Indian Institute of Technology, Indore, India

Email: rajneeshmisra@iiti.ac.in

#: Equal contribution

Abstract

Developing cost-effective and rational hole transporting materials is critical for fabricating high-performance perovskite solar cells (PSCs) and to promote their commercial endeavor. We have designed and developed pyridine (core) bridging diphenylamine-substituted carbazole (arm) small molecules, named as **2,6PyDANCBZ** and **3,5PyDANCBZ**. The linking topology of core and arm on their photophysical, thermal, semiconducting and photovoltaic properties were probed systematically. We found that the **2,6PyDANCBZ** shows higher mobility and conductivity along with uniform film-forming ability as compared to **3,5PyDANCBZ**. The PSCs fabricated with **2,6PyDANCBZ** supersede the performance delivered by Spiro-OMeTAD, and importantly also gave improved long-term stability. Our findings put forward small molecules based on core-arm linking topology for cost-effective hole selective layers designing.

Keywords: Carbazole, hole transport materials, perovskite solar cells, charge transport, electro-optical properties.

1. Introduction

Organic-inorganic hybrid perovskite solar cells (PSCs) have attracted tremendous interests due to their power conversion efficiency (PCE) soaring from 3.8% to 25.2% in a decade. These achievements are attributed to distinctive opto-electrical properties of organic-inorganic perovskites, such as suitable direct bandgap for sufficient utilization of solar energy and high charge mobility/long carrier diffusion length for effective photo-generated charge-carrier extraction and transportation.[1–5] In a typical PSC architect, perovskite layers are sandwiched between an electron / hole transporting material (ETM/HTM). Perovskite enjoys ambipolar characteristic, thus PSCs without hole selective layers can also be fabricated, but it is not adequate for the fabrication of high performance PSCs, as in perovskite the holes are at low level.[6] The HTMs play pivotal roles in facilitating holes extraction and transportation, and help to retard the degradation of PSCs induced by H_2O and oxygen. [7–10]

Currently, *2,2´,7,7´*-tetrakis-(*N*,*N*-di-p-methoxyphenylamine)-9,9´-spirobifluorene (Spiro-OMeTAD) is the most investigated HTM for PSCs fabrication due to its optimized recipe, ease of implementation to fabricate high performance devices. Kim and Seok et.al independently reported PSCs employing Spiro-OMeTAD as an effective HTM to yield >24% efficiency.[11,12] However, tedious synthesis process, expensive purification techniques, high cost, additional post-oxidation step, and low charge carrier mobility of Spiro-OMeTAD significantly limit its large-scale commercial endeavor. Alternatives, such as small-organic molecules, conjugated semi-conductive polymers, organometallic compounds, and inorganic *p*-type semiconductors, have been developed to replace Spiro-OMeTAD.[13–15] Among them, small-organic molecules attracted widespread attention due to the choice of molecular building blocks, tunable semiconducting properties, purification and minimum batch-to-batch variation.[16–19] A designed strategy to develop a rational molecule is a prevailing method to optimize and develop novel HTMs with excellent properties.

Various cores such as triazatruxene,[20] thiophene-based compounds,[21,22] and carbocyclic moieties[23] have been reported as HTMs,[14] but reports dealing with pyridine as a core for designing HTMs are scarce. The pyridine moiety in these HTM can act as a Lewis base and which in turn can assist defect passivation of perovskite and π-conjugation effect.[24–28] Besides the core of HTMs, the arm is also vital for optimizing the semiconducting properties of HTMs. Up to now, the bis(*N*^{3},*N*^{3},*N*^{6},*N*^{6}*-tetrakis(4-methoxyphenyl)-9H-carbazole-3,6-diamine*) (DANCBZ) moiety have been demonstrated to be a valuable arm for the designing of molecular HTMs owing to their superior charge-transporting ability, stability and low-cost.[29-36]

More importantly, linking topologies in molecular designing is an effective method to fine-tune electro-optical properties of materials.[37–41] For example, Sun *et al.* systemically studied the impact of linking topology of carbazole-based arm on basic properties, found that HTMs based on carbazole-based arm with 2,7-substitution display higher hole mobility and conductivity than that of HTMs with 3,6-substitution.[41] While linking topology of core and arm are vital to determine properties of HTMs via developing continuous π-conjugation between core and arm, and tuning dihedral angles of small molecules, trivial attention has been made to the linking topology effect of core and arm. For example, Lee and co-workers synthesized two types of deep-blue emitter: 26BTPIPy with *meta*-linking and 25BTPIPy with *para*-linking, the front, and the corresponding device showed excellent performance because of relatively planar structure leading to considerable overlapping of its frontier molecular orbitals.[38] Using core-arm type linking topology, HTMs based on thiophene-arylamine and pyrene-arylamine was investigated by Dai *et al*. and Wang *et al.*, respectively.[39,40] Considering arylamine-pyrene core-arm as an example, PYP16 with 1,6-arm substitution possessed reduced dihedral angles, lower level of planarity, improved film formation and polarized structure as compared to PYP27 with 2,7-arm substitution. By doing so, the devices with PYP16 presented higher efficiency and stability. To develop pyridine based HTMs and understanding the relationship between structural and chemical properties, and its influence on

device performance, we report the synthesis of two innovative molecules-based on pyridine as core which is end-capped with common DANCBZ as an arm. Such structures have not been designed and investigated to date. We further investigated the effect of the linking topology of core and arm on the properties of pyridine-based HTMs on the opto-electrical, thermal, semiconducting and photovoltaic properties in PSCs.

2. Results and discussion

2.1 Synthesis

The synthetic route for **2,6PyDANCBZ** and **3,5PyDANCBZ** is as outlined in **Scheme 1** and the details are described in the Supporting Information. N^3,N^3,N^6,N^6-tetrakis(4-methoxyphenyl)-9*H*-carbazole-3,6-diamine (**3**) was synthesized according to reported procedure.[42–44] The Buchwald–Hartwig amination reaction of **3** with **2,6-dibromopyridine** resulted in the final desired product 9,9'-(pyridine-2,6-diyl)bis(*N*3,*N*3,*N*6,*N*6-tetrakis(4-methoxyphenyl)-9H-carbazole-3,6-diamine) **2,6PyDANCBZ** with 46% yield. Similarly, the Buchwald–Hartwig amination reaction of **3** with **3,5-dibromopyridine** generated 9,9'-(pyridine-3,5-diyl)bis(*N*3,*N*3,*N*6,*N*6-tetrakis(4-methoxyphenyl)-9H-carbazole-3,6-diamine) **3,5PyDANCBZ** with 50% yield. The molecular structures of **2,6PyDANCBZ** and **3,5PyDANCBZ** were confirmed by various spectroscopic techniques such as ^{1}H, ^{13}C NMR spectroscopy and MALDI (supporting information). Both the small molecules are readily soluble in polar solvents such as dichloromethane, chloroform, ethyl acetate, 1,4-dioxane, *etc.*

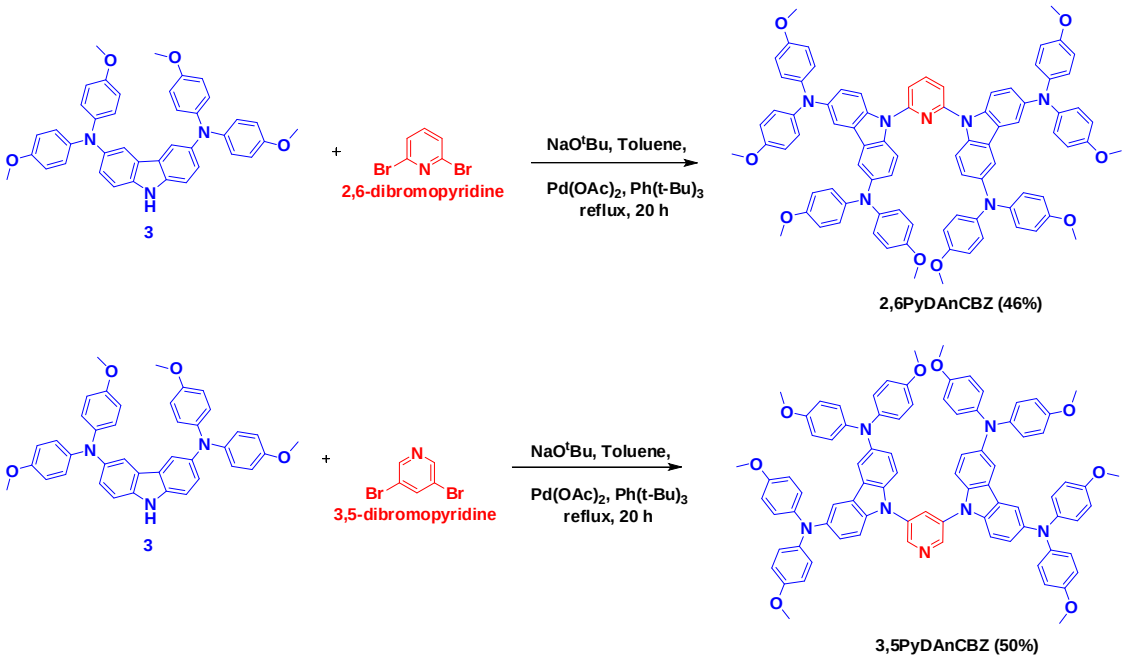

Scheme 1. Molecular structures and synthetic route of **2,6PyDANCBZ** and **3,5PyDANCBZ**.

2.2 Opto-electrical, thermal, semiconducting and photovoltaic properties

The normalized UV-vis absorption spectra of **2,6PyDANCBZ** and **3,5PyDANCBZ** in dichloromethane at room temperature were investigated (**Figure 1a**) and the data are compiled in **Table 1**. The absorption of **2,6PyDANCBZ** and **3,5PyDANCBZ** HTMs containing pyridine displayed a peak maximum at 309 and 308 nm, respectively, which is attributed to the π-π* electron transition of the large molecular conjugated system. The molecular structures of **2,6PyDANCBZ** and **3,5PyDANCBZ** exhibit absorption peaks in longer wavelength regions (350-400 nm) which could be due to the intramolecular charge transfer from donor to acceptor moieties. The relatively high intensity of shoulder band of **2,6PyDANCBZ** compared to that of **3,5PyDANCBZ** suggests that the **2,6PyDANCBZ** has a stronger charge transfer from the donor arm to the core acceptor unit. The onset absorption wavelengths (λ_{onset}, around 440 nm) of **2,6PyDANCBZ** and **3,5PyDANCBZ** are presented here. The optical bandgap (E_g^{opt}) of **2,6PyDANCBZ** and **3,5PyDANCBZ** were calculated to be around 2.82 eV from the equation ($E_g^{opt} = 1240/\lambda_{onset.}$). The highest occupied molecular orbital energy level (E_{HOMO}) of

2,6PyDANCBZ and **3,5PyDANCBZ** were evaluated by cyclic voltammetry (Figure 1b). Both **2,6PyDANCBZ** and **3,5PyDANCBZ** exhibit reversible cyclic voltammogram and the oxidation cycle contain two reversible oxidation potentials corresponding to the formation of the radical cation of the carbazole moiety and the dication quinonediimine, respectively.[45] The corresponding E_{HOMO} values were estimated from the half-wave oxidation value ($E^{1/2}_{ox}$) of the first oxidation waves, considering 0.67 eV versus a normal hydrogen electrode (NHE) and 4.44 eV versus vacuum, by using the equation $E_{HOMO} = (E^{1/2}_{ox} + 0.67 + 4.44)$ eV and the data are summarized in Table 1.[40-46] Both the samples **2,6PyDANCBZ** and **3,5PyDANCBZ** exhibited similar E_{HOMO} level of – 5.5 eV. The lowest unoccupied molecular orbital energy level (E_{LUMO}) was calculated from the equation ($E_{LUMO} = E_{HOMO} + E_g^{opt}$) to be – 2.7 eV. Figure S1a shows the energy level diagram of fabricated device, where valence and conduction band of mixed-cation perovskite films is -5.9 and -4.4 eV, respectively,[47] illustrating that the presented HTMs are energetically favourable for hole transportation. More importantly, the large energy barrier between the conduction band of perovskite and E_{LUMO} of HTMs could efficiently block the undesired photo-generated electron transfer and particularly decrease charge recombination rate at the perovskite/HTM interface. The thermal stability of HTMs were evaluated by employing differential scanning calorimetry (DSC) measurements (Figure 1c and Figure S2). The **2,6PyDANCBZ** and **3,5PyDANCBZ** exhibit a high glass transition temperature (T_g) of 132 and 126 °C, respectively, which are higher than that of Spiro-OMeTAD.[48] The notable high T_g shown by HTMs will prevent any phase change process, suggesting the functioning of devices in the temperature window required for commercial validation.

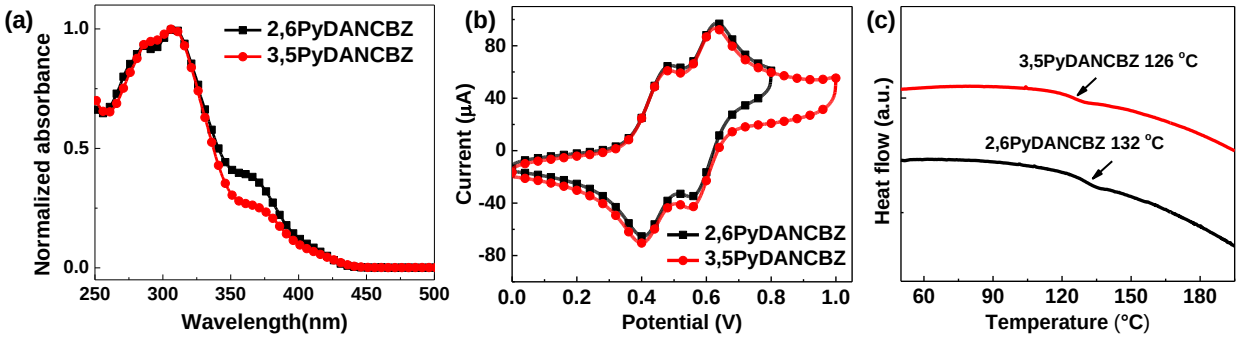

Figure 1. (a) Normalized UV-Vis absorption spectra of **2,6PyDANCBZ** and **3,5PyDANCBZ** in dichloromethane. (b) Cyclic voltammetry of **2,6PyDANCBZ** and **3,5PyDANCBZ** materials. (c) Differential scanning calorimetry of seconding heating curves of **2,6PyDANCBZ** and **3,5PyDANCBZ** materials.

Table 1. Photophysical, thermal, and semiconducting characteristics of the new **2,6PyDANCBZ** and **3,5PyDANCBZ**.

HTM	$\lambda_{max}/\lambda_{onset}$ (nm)	E_g (eV)	E_{HOMO} (eV)	E_{LUMO} (eV)	T_g (°C)	Conductivity (μS cm^{-1})	Mobility (10^{-5} cm^2 V^{-1} s^{-1})[d]
2,6PyDANCBZ	284/309/440	2.82[a]/3.30[b]	-5.5[a]/-4.28[b]	-2.7[c]/-0.98[b]	132	3.9	16
3,5PyDANCBZ	287/308/440	2.82[a]/3.26[b]	-5.5[a]/-4.34[b]	-2.7[c]/-1.08[b]	126	3.1	9

[a]E_{HOMO} is estimated with $E^{1/2}{}_{ox}$ versus the ferrocene redox couple (Fc/Fc^+) + 0.67 eV versus a normal hydrogen electrode (NHE; + 4.44 eV versus vacuum); [b]DFT calculations of HTMs: $E_{LUMO}=E_{HOMO}+E_g$; [c]$E_{LUMO}=E_{HOMO}+E_g$, and E_{HOMO} and E_g estimated from the redox potential in cyclic voltammetry and UV–vis absorption spectra, respectively; [d]HTMs without dopant.

We study the influence of linking topology of these HTMs on electrical properties, such as conductivity and charge carrier mobility. The conductivity (σ_0) was determined by measuring the linear current density-voltage (*J-V*) curve of the device in a simple structure (ITO/HTM/Ag) and calculated by the equation of $\sigma_0=JdV^{-1}$. The *J-V* curves was tested under the dark and ambient condition as shown in **Figure 2a**. The conductivity values of undoped **2,6PyDANCBZ** and **3,5PyDANCBZ** were ~ 3.7 and 3.1 μS cm^{-1}, these values increases to 5.5 and 4.7 μS cm^{-1} in the case of doped **2,6PyDANCBZ** and **3,5PyDANCBZ**, respectively. We noted slightly higher

conductivity of both **2,6-Py** and **3,5-Py** substituted based HTM in doped form. Space charge limited current (SCLC) method was used to evaluate hole mobility of the synthesized HTMs using hole-only device structure of ITO/PEDOT:PSS/HTM/Ag and *J-V* curves were tested under the dark and ambient condition as shown in **Figure 2b**. The hole mobility values of HTMs were calculated from the slope of the $J^{1/2}$–V curves (Figure S3) according to Mott-Gurney law ($J=9\varepsilon\varepsilon_0\mu V_{app}^2/8L^3$) and the data were collected in Table 1. The calculated hole mobility values of undoped **2,6-Py** and **3,5-Py** substituted HTM were 1.6×10^{-4} and 0.9×10^{-4} cm^2 V^{-1} s^{-1}, and doped **2,6-Py** and **3,5-Py** substituted HTM showed the increased mobility values of 2.0×10^{-4} and 1.2×10^{-4} cm^2 V^{-1} s^{-1}, respectively, which are higher than that of the doped Spiro-OMeTAD (< 5×10^{-5} cm^2 V^{-1} s^{-1}) reported.[24,48,49] The conductivities and mobilities values of 2,6PyDANCBZ are higher than of **3,5PyDANCBZ**, in both doped as well as undoped form.

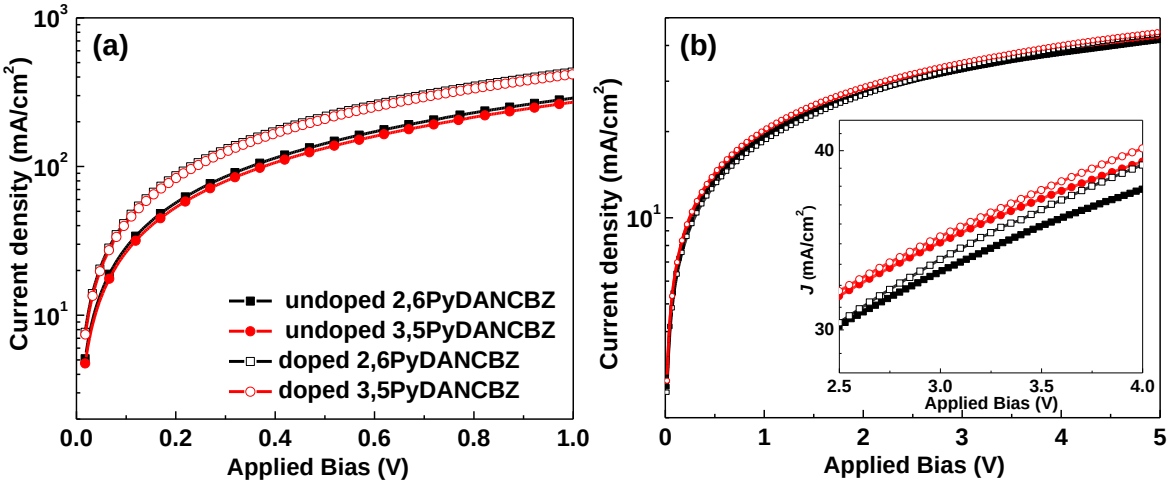

Figure 2. a) *J-V* curves from conductivity measurements (device structure: ITO/HTM/Ag) of the small molecules, b) The *J-V* curves of the **2,6PyDANCBZ** and **3,5PyDANCBZ** HTM based hole-only device with structure: ITO/PEDOT:PSS/HTM/Ag. The inset depicts the enhancement in the current after doping.

To gain insight into the structural and electronic properties difference of the **2,6PyDANCBZ** and **3,5PyDANCBZ** compounds, density functional theory (DFT) calculations were performed at

the B3LYP/6-31G(d) level. The calculated frontier molecular orbitals are depicted in **Figure 3a** and the values are compiled in Table 1. The E_{HOMO} level is localized at donor DANCBZ unit (arm) of pyridine-based HTMs, while the E_{LUMO} level is localized on acceptor pyridine unit (core). Especially, the E_{HOMO} and E_{LUMO} energy levels of **3,5PyDANCBZ** are slightly stabilized as compared to E_{HOMO} and E_{LUMO} energy levels of **2,6PyDAnCBZ**. The theoretical determined E_{HOMO} levels of **2,6PyDANCBZ** and **3,5PyDANCBZ** are – 4.28 eV and – 4.34 eV whereas E_{LUMO} levels are – 0.98 eV and – 1.08 eV, respectively. The HOMO and LUMO are well separated allowing distinct intra-molecular charge transfer from the donor DAnCBZ arm to the acceptor pyridine core. In order to investigate the influence of linking topology on molecular structure, we calculate the representative dihedral angles between the pyridine core and DANCBZ arm. As shown (Figure 3b), the **2,6PyDANCBZ** with 56.76° and 35.95° dihedral angles owns a lower level of planarity as compared to **3,5PyDANCBZ** with 46.61° and 38.58° dihedral angles, which reduces the molecular stacking and helps in the formation of uniform film in **2,6PyDANCBZ**.[50,51]

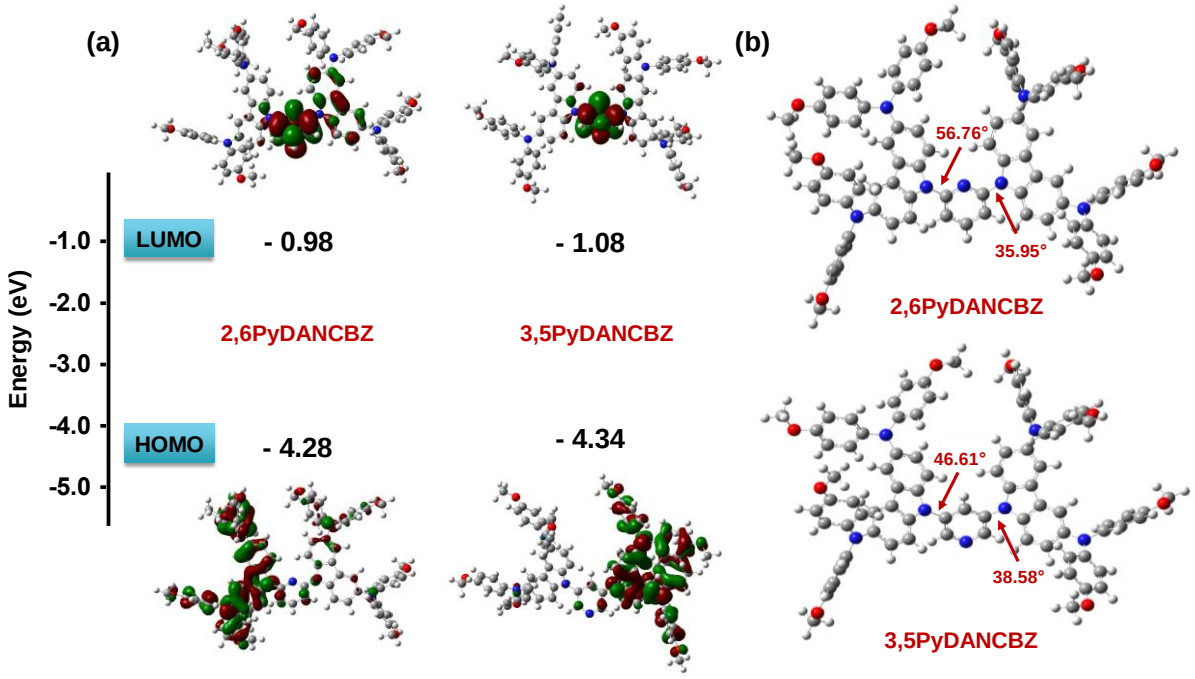

Figure 3. a) Energy level diagram showing the HOMO and LUMO levels of **2,6PyDANCBZ** and **3,5PyDANCBZ** as determined at the B3LYP/6-31G(d) level and b) dihedral angles of the **2,6PyDANCBZ** and **3,5PyDANCBZ** materials.

The film-forming abilities of the HTMs were investigated and perovskite/**2,6PyDANCBZ** represents uniform microstructure while perovskite/**3,5PyDANCBZ** showed pin-holes, which can also be visualized by the naked eye (**Figure 4a**). Surface top view images acquired through scanning electron microscopy (SEM) experiments of the perovskite covered with different HTMs are illustrated in Figure 4b and 4c. It can be deducted that the perovskite/**3,5PyDANCBZ** film with pinholes and voids was rougher than perovskite/**2,6PyDANCBZ**. Arguably, the smooth nature of **2,6PyDANCBZ** film will enhance the interfacial contact between the perovskite and HTM layer, avoid direct contact of perovskite with electrode and improve the performance of corresponding devices. Our results suggest that the linking topology on core and arm can significantly affect the film-forming abilities, although these HTMs have similar photophysical, electrochemical, thermal and electrical properties.

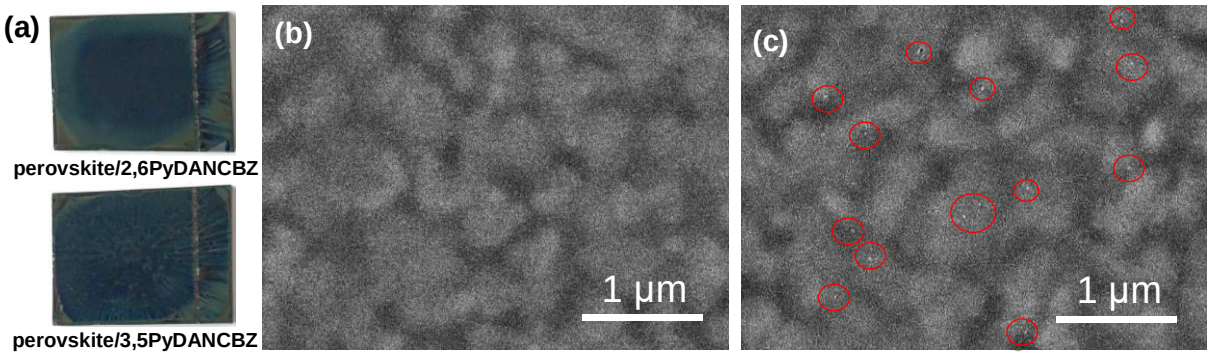

Figure 4. a) Visual image of perovskite covered with **2,6PyDANCBZ** and **3,5PyDANCBZ** films, b) SEM images of perovskite with **2,6PyDANCBZ** and c) **3,5PyDANCBZ**.

2.2 Device performance

To elucidate the influence of side arm of HTM on the performance of PSCs, we fabricated planar devices with an architect of ITO/SnO_2/perovskite/HTM/Au, introducing **2,6PyDANCBZ**, **3,5PyDANCBZ** and Spiro-OMeTAD as HTMs. Device schematic with HTM is shown in Figure S1b.[7,8] The cross-sectional SEM image of devices with **2,6PyDANCBZ** and **3,5PyDANCBZ** (**Figure 5a** and 5b) depicts a stacked structure, having a ~ 440 nm-thick perovskite film, and a thick film 127 nm of **2,6PyDANCBZ** and 113 nm of **3,5PyDANCBZ** film, respectively. Figure

5c and 5d illustrate the *J-V* curves of the PSCs fabricated with developed HTMs under AM 1.5G illumination (100 mW cm^{-2}), and the detailed photovoltaic (PV) parameters data are summarized in **Table 2**. The best device employing **2,6PyDANCBZ** under reverse voltage scan yields a high PCE of 17.78%, with a V_{oc} of 1061 mV, a short-circuit current (J_{sc}) of 22.13 mA cm^{-2} and a fill factor (*FF*) of 75.7%, while the device with **3,5PyDANCBZ** gave a relatively lower PCE of 15.92%, with a V_{oc} of 1043 mV, a J_{sc} of 22.88 mA cm^{-2} and a *FF* of 66.7%. Expectedly, **3,5PyDANCBZ** yielded a lower PCE than **2,6PyDANCBZ** and this is ascribed to its high electrical properties and favourable microstructures. Subsequently, it also gave enhanced *FF* due to higher conductivity of the doped **2,6 Py** than **3,5-Py** substituted one, thus decreasing the series resistance of the film. The series resistance (R_s) and shunt resistance (R_{sh}) of **2,6PyDANCBZ** and **3,5PyDANCBZ** were shown in Table 2. The **2,6PyDANCBZ**-based device showed the lower R_s and higher R_{sh} of 27.8 Ω and 33.9 kΩ (*J-V* curves in RS condition), whereas **3,5PyDANCBZ** showed R_s and R_{sh} of 41.0 Ω and 12.2 kΩ, respectively. Subsequently, **2,6PyDANCBZ** yielded improved PCE with high FF, which is due to the lower R_s and higher R_{sh}.[16,52] Besides, the rough microstructure of **3,5-Py** substituted HTM leads to unfavourable interfacial contact, which also lowers the *FF*. The average and detailed PV parameters are summarized in Table S1 and S2. To evaluate the performance of the devices with different HTMs, the stabilized power output tracking was evaluated and were 17.7% and 13.1% for PSCs based on **2,6PyDANCBZ** and **3,5PyDANCBZ**, respectively (Figure 5g), consistent with the *J-V* curves. The Spiro-OMeTAD-based device under the same condition gave a PCE of 17.08% with a V_{oc} of 1053 mV, J_{sc} of 21.63 mA cm^{-2} and a *FF* of 75.0% (Figure 5e). The relatively high performance of **2,6PyDANCBZ**-based device is in accordance with the improved semiconducting properties and aligned energy level. Figure 5f presents the external quantum efficiency (EQE) spectra and the integrated current density of corresponding PSCs. The integrated current density values of PSCs with **2,6PyDANCBZ**, **3,5PyDANCBZ** and Spiro-OMeTAD are 21.73, 21.62 and 21.16 mA cm^{-2},

respectively, which are in agreement with the J_{sc} value measured under the standard solar AM 1.5G.

The hysteresis index (*HI*) in devices was studied via measuring the *J-V* in the forward scan (FS) and reverse scan (RS) direction. The **2,6PyDANCBZ**-based device gave low *HI* (0.033) as compared to Spiro-OMeTAD (0.060), the HI was calculated according to the following equation:

$$HI = [J_{RS}(0.8V_{oc})\text{-}J_{FS}(0.8V_{oc})]/J_{RS}(0.8V_{oc}).^{10,53}$$

3,5PyDANCBZ-based PSC with slightly high *HI* (0.305) can be attributed to poor uniformity. Notably, PSCs with **2,6PyDANCBZ** presented improved performance than of Spiro-OMeTAD, suggesting its potential as a cost-effective replacement. By further interface optimization and perovskites components tuning, we believe that the PCE of **2,6PyDANCBZ-**based PSCs can be substantially improved to achieve state of the art. Further, we have also fabricated the inverted PSCs with architecture (ITO/HTM/perovskite/$PC_{61}BM$/BCP/Ag). The device performance with different HTMs was shown in Figure 5h and Table S3 and the PCE of the PSCs with **2,6PyDANCBZ** and **3,5PyDANCBZ** are 10.79% and 10.18%, respectively, which is comparable with those of classical PEDOT:PSS (10.66%). Suggesting the suitability of **2,6PyDANCBZ** as a competitive candidate to supersede the conventional Spiro-OMeTAD.

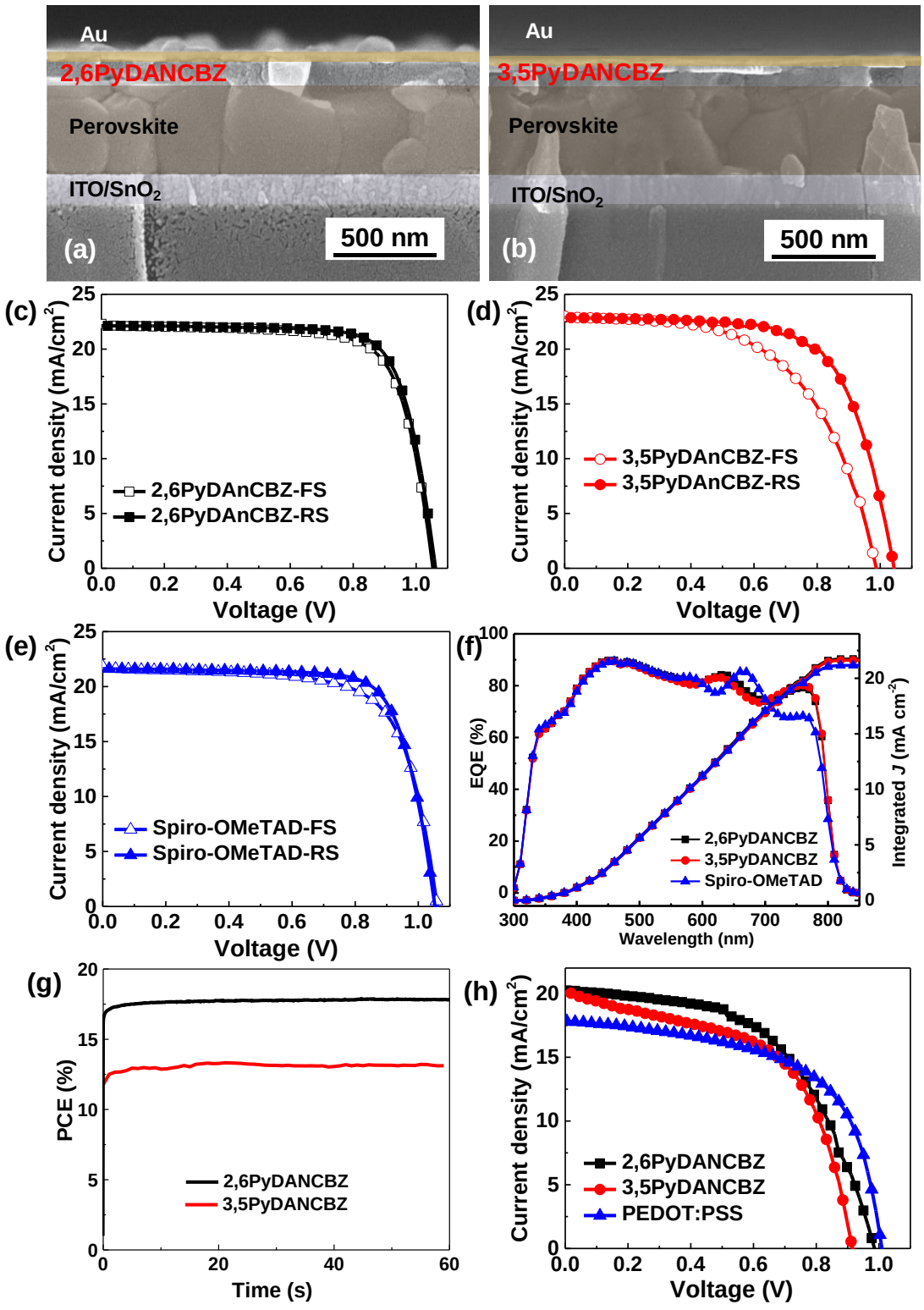

Figure 5. Cross-sectional SEM images of the PSCs with a) **2,6PyDANCBZ** and b) **3,5PyDANCBZ**; *J-V* hysteresis curves of forward and reverse scans under simulated AM 1.5G illumination for the champion *n-i-p* devices with different HTMs, c) **2,6PyDANCBZ**, d) **3,5PyDANCBZ** and e) Spiro-OMeTAD, (f) EQE curves of corresponding PSCs (*n-i-p*), g) The

stabilized power output of PSCs with **2,6PyDANCBZ** and **3,5PyDANCBZ** and h) *J-V* curves of the inverted-structure (*p-i-n*) devices with different HTMs.

Table 2. Photovoltaic parameters of the PSCs with different HTMs.

HTMs	direction	V_{oc} (mV)	J_{sc} (mA cm^{-2})	FF (%)	PCE (%)	R_s (Ω)	R_{sh} (kΩ)	*HI*
2,6PyDANCBZ	FS	1053	22.20	73.4	17.16	28.6	7.6	0.033
2,6PyDANCBZ	RS	1061	22.13	75.7	17.78	27.8	33.9	
3,5PyDANCBZ	FS	987	22.95	56.5	12.78	49.3	5.0	0.305
3,5PyDANCBZ	RS	1043	22.88	66.7	15.92	41.0	12.2	
Spiro-OMeTAD	FS	1060	21.69	69.8	16.05	27.9	5.8	0.060
Spiro-OMeTAD	RS	1053	21.63	75.0	17.08	31.7	18.0	

[a]R_s and R_{sh} of PSCs with different HTMs were estimated by slope of the *J-V* curves near V_{oc} and J_{sc}, respectively.

Electrical impedance spectroscopy (EIS) analysis was conducted to understand the charge transport mechanisms (interface recombination, diffusion, *etc.*) of devices with pyridine-based HTMs. Figure S4a,b showed the typical Nyquist (Z´ – Z´´) and Bode (a´ and b´) plots of impedance spectroscopy for the studied configurations under illumination for different photovoltages. An equivalent circuit was used to extract information about recombination processes as shown in Figure S4a. The resistance and capacitance values are represented in **Figure 6.** From the equivalent circuit used we derived the resistance and capacitance value, and noted variance in the slope in the recombination *vs* voltage graph. This can be explained by the calculation of the ideality factor (n=1/β).[54] The PSCs with **2,6PyDANCBZ** and **3,5PyDANCBZ** presented β values of 0.26 and 0.29, respectively, and the ideality factor increases from 3.45 to 3.85 when **2,6PyDANCBZ** was substituted with **3,5PyDANCBZ**, suggesting **2,6PyDANCBZ** based PSCs reduces the recombination process as compared to **3,5PyDANCBZ**. Furthermore, **2,6PyDANCBZ** based PSCs illustrated lower capacitance value compared to **3,5PyDANCBZ**. The relatively higher ideality factor and lower capacitance values of **2,6PyDANCBZ**-based PSCs will allow to improve charge transportation ability and thus enhanced performance of PSCs.[55,56]

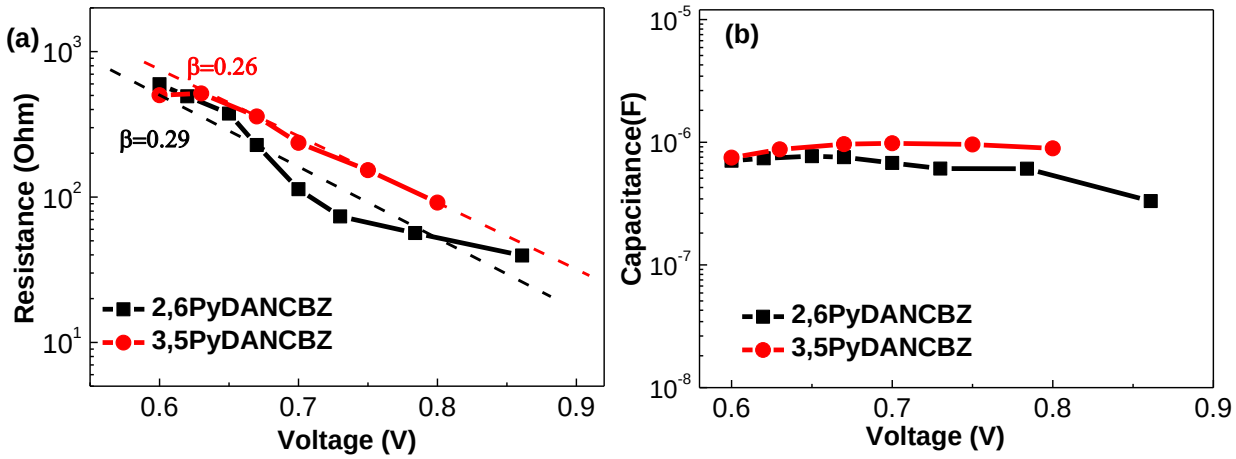

Figure 6. a) Resistance and b) capacitance plots for **2,6PyDANCBZ** and **3,5PyDANCBZ**-based PSCs. Derived from the fitting of impedance spectroscopy spectra at different illumination intensities through open-circuit regime.

We studied the long-term stability of PSCs with different HTMs. The un-encapsulated devices were stored in a dry box (40-50% relative humidity, room temperature) and measured in an ambient condition. The PCE values of the devices with **2,6PyDANCBZ** and **3,5PyDANCBZ** maintained at 79.6% and 75.6% of their initial values after 5,500 h, respectively (**Figure 7**). In contrast, the performance of PSCs with Spiro-OMeTAD degraded to 70.5% of its initial value during this time. The result demonstrates PSCs with pyridine based HTMs shows improved device stability as compared to Spiro-OMeTAD. The plausible reasons for improved stability are as follows: the perovskite/**2,6PyDANCBZ** and perovskite/**3,5PyDANCBZ** show a higher water contact angle of 91^{o} and 86^{o} compared to that of Spiro-OMeTAD (76^{o}), the excellent hydrophobic nature of developed HTMs can effectively block the water penetration into perovskite layers. Another supporting explanation is that the pyridine core of HTMs acts as a passivating agent for the perovskite layer and perovskite/HTM interface. [57–59]

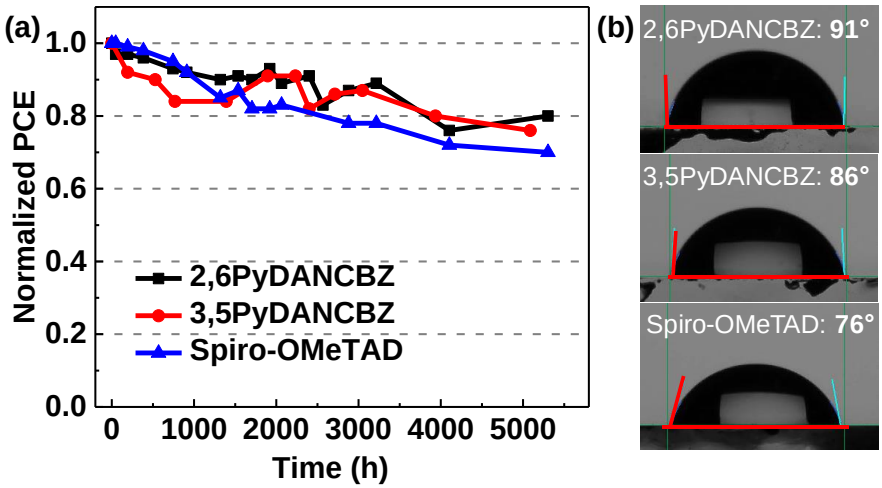

Figure 7. Plots of normalized PCE of a) PSCs with different HTMs *vs* the storage time and b) contact angle of perovskite with different HTMs.

Developing cost-effective HTMs with excellent properties is an effective methodology to lower the cost of PSCs modules to promote the commercialization.[60] Our results suggest that the pyridine based HTMs are competitive candidates for high-performance PSCs fabrication. The cost of laboratory synthesis and purification of **2,6PyDANCBZ** and **3,5PyDANCBZ** is estimated, and the detailed cost calculations are shown in the supporting information. The cost of **2,6PyDANCBZ** and **3,5PyDANCBZ** is about 28.1 € and 27.0 € per gram, respectively, which is significantly lower than that of Spiro-OMeTAD (~ 400 € per gram, Sigma-Aldrich). Additionally, the optimal concentration of **2,6PyDANCBZ** (39.6 mg mL^{-1}) was almost half of Spiro-OMeTAD solution (72.3 mg mL^{-1}), this will further allow to achieve lower the material cost during device fabrication. (1.11 € per mL of 2,6PyDANCBZ *vs* 21.7 € per mL of Spiro-OMeTAD solution), suggesting the usage of **2,6PyDANCBZ** as a promising candidate for hole extraction materials.[13]

3. Conclusion

We have designed pyridine bridging diphenylamine-carbazole as hole transporting layers for PSCs. We systematically investigated the core-arm linking topology on the optical and electronic properties of developed HTMs. Our results suggest that the **2,6PyDANCBZ** display higher

conductivity due to stronger charge transfer from the donor arm to the core of the acceptor, and uniform film-forming ability. As compared to **3,5PyDANCBZ**, the fabricated PSCs with **2,6Py** substitution showed improved performance when integrated into PSCs, and supersede the performance of conventional Spiro-OMeTAD. Our results put forward new design strategies for cost-effective and efficient hole transport materials, and also provide the guiding principle on the molecular design of core-arm linking topology.

Author Contributions

P.H. made the experiments, fabricated the devices and prepared the initial draft, Manju synthesized the molecules and made chemical analysis, S.K. performed all the electro-optical measurements, G.S. performed DFT calculation, M.S. performed impedance spectroscopy, R.M. supervised the work of Manju and G.S. and analyse the data, S.A. supervised and directed the research.

Conflicts of interest

The authors declare no conflict of interest.

Acknowledgments

This work has received funding from the European Union H2020 Programme under European Research council Consolidator grant [MOLEMAT, 726360]. This work was supported by the DST, (DST/TMD/SERI/D05(C)), INSA (SP/YSP/139/2017/2293), SERB CRG/2018/000032 and CSIR 01(2934)/18/EMR-II. M.S. thanks the National Research grant "Juan de la Cierva" [FJCI-2017-31761]. We are grateful to the Sophisticated Instrumentation Centre (SIC), Indian Institute of Technology (IIT), Indore. Manju thanks CSIR Delhi for fellowship.

Supporting Information

Device fabrication and characterization methodology, general experimental methods and ^{1}H and ^{13}C NMR and HRMS spectra of the developed compounds, cost calculations.

References

(1) Kojima, A.; Teshima, K.; Shirai, Y.; Miyasaka, T. Organometal Halide Perovskites as Visible-Light Sensitizers for Photovoltaic Cells. *J. Am. Chem. Soc.* **2009**, *131* (17), 6050–6051.

(2) Burschka, J.; Pellet, N.; Moon, S.-J. J.; Humphry-Baker, R.; Gao, P.; Nazeeruddin, M. K.; Grätzel, M. Sequential Deposition as a Route to High-Performance Perovskite-Sensitized Solar Cells. *Nature* **2013**, *499* (7458), 316–319.

(3) NREL, Best Research-Cell Efficiencies. *https://www.nrel.gov/pv/cell-efficiency.html* (accessed: March 2020).

(4) Liu, M.; Johnston, M. B.; Snaith, H. J. Efficient Planar Heterojunction Perovskite Solar Cells by Vapour Deposition. *Nature* **2013**, *501* (7467), 395–398.

(5) Kim, H.-S.; Lee, C.-R.; Im, J.-H.; Lee, K.-B.; Moehl, T.; Marchioro, A.; Moon, S.-J.; Humphry-Baker, R.; Yum, J.-H.; Moser, J. E.; Grätzel, M.; Park, N.-G. Lead Iodide Perovskite Sensitized All-Solid-State Submicron Thin Film Mesoscopic Solar Cell with Efficiency Exceeding 9%. *Sci. Rep.* **2012**, *2* (1), 591.

(6) Zhang, H.; Wang, H.; Williams, S. T.; Xiong, D.; Zhang, W.; Chueh, C.-C. C.; Chen, W.; Jen, A. K. Y. K.-Y. SrCl2 Derived Perovskite Facilitating a High Efficiency of 16% in Hole-Conductor-Free Fully Printable Mesoscopic Perovskite Solar Cells. *Adv. Mater.* **2017**, *29* (15), 1606608.

(7) Huang, P.; Yuan, L.; Zhang, K.; Chen, Q.; Zhou, Y.; Song, B.; Li, Y. Room-Temperature and Aqueous Solution-Processed Two-Dimensional TiS_2 as an Electron Transport Layer for Highly Efficient and Stable Planar n–i–p Perovskite Solar Cells. *ACS Appl. Mater. Interfaces* **2018**, *10* (17), 14796–14802.

(8) Huang, P.; Chen, Q.; Zhang, K.; Yuan, L.; Zhou, Y.; Song, B.; Li, Y. 21.7% Efficiency Achieved in Planar n–i–p Perovskite Solar Cells via Interface Engineering with Water-

Soluble 2D TiS 2. *J. Mater. Chem. A* **2019**, *7* (11), 6213–6219.

(9) Jung, E. H.; Jeon, N. J.; Park, E. Y.; Moon, C. S.; Shin, T. J.; Yang, T.-Y.; Noh, J. H.; Seo, J. Efficient, Stable and Scalable Perovskite Solar Cells Using Poly(3-Hexylthiophene). *Nature* **2019**, *567* (7749), 511–515.

(10) Caliò, L.; Salado, M.; Kazim, S.; Ahmad, S. A Generic Route of Hydrophobic Doping in Hole Transporting Material to Increase Longevity of Perovskite Solar Cells. *Joule* **2018**, *2* (9), 1800–1815.

(11) Kim, M.; Kim, G.-H.; Lee, T. K.; Choi, I. W.; Choi, H. W.; Jo, Y.; Yoon, Y. J.; Kim, J. W.; Lee, J.; Huh, D.; Lee, H.; Kwak, S. K.; Kim, J. Y.; Kim, D. S. Methylammonium Chloride Induces Intermediate Phase Stabilization for Efficient Perovskite Solar Cells. *Joule* **2019**, *3* (9), 2179–2192.

(12) Min, H.; Kim, M.; Lee, S.-U.; Kim, H.; Kim, G.; Choi, K.; Lee, J. H.; Seok, S. Il. Efficient, Stable Solar Cells by Using Inherent Bandgap of α-Phase Formamidinium Lead Iodide. *Science.* **2019**, *366* (6466), 749–753.

(13) Calió, L.; Kazim, S.; Grätzel, M.; Ahmad, S. Hole-Transport Materials for Perovskite Solar Cells. *Angew. Chemie - Int. Ed.* **2016**, *55* (47), 14522–14545; *Angew. Chemie.*, 2016, 128, 14740-14764.

(14) Urieta-Mora, J.; García-Benito, I.; Molina-Ontoria, A.; Martín, N. Hole Transporting Materials for Perovskite Solar Cells: A Chemical Approach. *Chem. Soc. Rev.* **2018**, *47* (23), 8541–8571.

(15) Gangala, S.; Misra, R. Spiro-Linked Organic Small Molecules as Hole-Transport Materials for Perovskite Solar Cells. *J. Mater. Chem. A* **2018**, *6* (39), 18750–18765.

(16) Shen, C.; Wu, Y.; Zhang, H.; Li, E.; Zhang, W.; Xu, X.; Wu, W.; Tian, H.; Zhu, W.-H. Semi-Locked Tetrathienylethene as a Building Block for Hole-Transporting Materials: Toward Efficient and Stable Perovskite Solar Cells. *Angew. Chemie Int. Ed.* **2019**, *58*

(12), 3784–3789.

(17) Yin, X.; Zhou, J.; Song, Z.; Dong, Z.; Bao, Q.; Shrestha, N.; Bista, S. S.; Ellingson, R. J.; Yan, Y.; Tang, W. Dithieno[3,2-b:2′,3′-d]Pyrrol-Cored Hole Transport Material Enabling Over 21% Efficiency Dopant-Free Perovskite Solar Cells. *Adv. Funct. Mater.* **2019**, 1904300.

(18) Xu, L.; Huang, P.; Zhang, J.; Jia, X.; Ma, Z.; Sun, Y.; Zhou, Y.; Yuan, N.; Ding, J. N , N -Di- Para -Methylthiophenylamine-Substituted (2-Ethylhexyl)-9 H -Carbazole: A Simple, Dopant-Free Hole-Transporting Material for Planar Perovskite Solar Cells. *J. Phys. Chem. C* **2017**, *121* (40), 21821–21826.

(19) Zhang, J.; Xu, L. J.; Huang, P.; Zhou, Y.; Zhu, Y. Y.; Yuan, N. Y.; Ding, J. N.; Zhang, Z. G.; Li, Y. F. A Simple and Dopant-Free Hole-Transporting Material Based on (2-Ethylhexyl)-9 H -Carbazole for Efficient Planar Perovskite Solar Cells. *J. Mater. Chem. C* **2017**, *5* (48), 12752–12757.

(20) Rakstys, K.; Abate, A.; Dar, M. I.; Gao, P.; Jankauskas, V.; Jacopin, G.; Kamarauskas, E.; Kazim, S.; Ahmad, S.; Grätzel, M.; Nazeeruddin, M. K. Triazatruxene-Based Hole Transporting Materials for Highly Efficient Perovskite Solar Cells. *J. Am. Chem. Soc.* **2015**, *137* (51), 16172–16178.

(21) Zhang, F.; Wang, Z.; Zhu, H.; Pellet, N.; Luo, J.; Yi, C.; Liu, X.; Liu, H.; Wang, S.; Li, X.; Xiao, Y.; Zakeeruddin, S. M.; Bi, D.; Grätzel, M. Over 20% PCE Perovskite Solar Cells with Superior Stability Achieved by Novel and Low-Cost Hole-Transporting Materials. *Nano Energy* **2017**, *41*, 469–475.

(22) García-Benito, I.; Zimmermann, I.; Urieta-Mora, J.; Aragó, J.; Molina-Ontoria, A.; Ortí, E.; Martín, N.; Nazeeruddin, M. K. Isomerism Effect on the Photovoltaic Properties of Benzotrithiophene-Based Hole-Transporting Materials. *J. Mater. Chem. A* **2017**, *5* (18), 8317–8324.

(23) Malinauskas, T.; Saliba, M.; Matsui, T.; Daskeviciene, M.; Urnikaite, S.; Gratia, P.; Send, R.; Wonneberger, H.; Bruder, I.; Graetzel, M.; Getautis, V.; Nazeeruddin, M. K. Branched Methoxydiphenylamine-Substituted Fluorene Derivatives as Hole Transporting Materials for High-Performance Perovskite Solar Cells. *Energy Environ. Sci.* **2016**, *9* (5), 1681–1686.

(24) Liu, X.; Ma, S.; Ding, Y.; Gao, J.; Liu, X.; Yao, J.; Dai, S. Molecular Engineering of Simple Carbazole-Triphenylamine Hole Transporting Materials by Replacing Benzene with Pyridine Unit for Perovskite Solar Cells. *Sol. RRL* **2019**, 1800337.

(25) Xu, B.; Zhu, Z.; Zhang, J.; Liu, H.; Chueh, C. C.; Li, X.; Jen, A. K. Y. 4-Tert-Butylpyridine Free Organic Hole Transporting Materials for Stable and Efficient Planar Perovskite Solar Cells. *Adv. Energy Mater.* **2017**, 1700683.

(26) Reddy, S. S.; Arivunithi, V. M.; Sree, V. G.; Kwon, H.; Park, J.; Kang, Y. C.; Zhu, H.; Noh, Y. Y.; Jin, S. H. Lewis Acid-Base Adduct-Type Organic Hole Transport Material for High Performance and Air-Stable Perovskite Solar Cells. *Nano Energy* **2019**, *58*, 284–292.

(27) Duan, L.; Chen, Y.; Jia, J.; Zong, X.; Sun, Z.; Wu, Q.; Xue, S. Dopant-Free Hole-Transport Materials Based on 2,4,6-Triarylpyridine for Inverted Planar Perovskite Solar Cells. *ACS Appl. Energy Mater.* **2020**, *3* (2), 1672–1683.

(28) Wu, F.; Shan, Y.; Qiao, J.; Zhong, C.; Wang, R.; Song, Q.; Zhu, L. Replacement of Biphenyl by Bipyridine Enabling Powerful Hole Transport Materials for Efficient Perovskite Solar Cells. *ChemSusChem* **2017**, *10* (19), 3833–3838.

(29) Xu, B.; Sheibani, E.; Liu, P.; Zhang, J.; Tian, H.; Vlachopoulos, N.; Boschloo, G.; Kloo, L.; Hagfeldt, A.; Sun, L. Carbazole-Based Hole-Transport Materials for Efficient Solid-State Dye-Sensitized Solar Cells and Perovskite Solar Cells. *Adv. Mater.* **2014**, *26* (38), 6629–6634.

(30) Lu, C.; Choi, I. T.; Kim, J.; Kim, H. K. Simple Synthesis and Molecular Engineering of Low-Cost and Star-Shaped Carbazole-Based Hole Transporting Materials for Highly Efficient Perovskite Solar Cells. *J. Mater. Chem. A* **2017**, *5* (38), 20263–20276.

(31) Zhang, M. D.; Zheng, B. H.; Zhuang, Q. F.; Huang, C. Y.; Cao, H.; Chen, M. D.; Wang, B. Two Dimethoxyphenylamine-Substituted Carbazole Derivatives as Hole-Transporting Materials for Efficient Inorganic-Organic Hybrid Perovskite Solar Cells. *Dye. Pigment.* **2017**, *146*, 589–595.

(32) Ji, Y.; He, B.; Lu, H.; Xu, J.; Wang, R.; Jin, Y.; Zhong, C.; Shan, Y.; Wu, F.; Zhu, L. Core Structure Engineering in Hole-Transport Materials to Achieve Highly Efficient Perovskite Solar Cells. *ChemSusChem* **2019**, *12* (7), 1374–1380.

(33) Kang, M. S.; Sung, S. Do; Choi, I. T.; Kim, H.; Hong, M.; Kim, J.; Lee, W. I.; Kim, H. K. Novel Carbazole-Based Hole-Transporting Materials with Star-Shaped Chemical Structures for Perovskite-Sensitized Solar Cells. *ACS Appl. Mater. Interfaces* **2015**, *7* (40), 22213–22217.

(34) Sung, S. Do; Kang, M. S.; Choi, I. T.; Kim, H. M.; Kim, H.; Hong, M.; Kim, H. K.; Lee, W. I. 14.8% Perovskite Solar Cells Employing Carbazole Derivatives as Hole Transporting Materials. *Chem. Commun.* **2014**, *50* (91), 14161–14163.

(35) Gratia, P.; Magomedov, A.; Malinauskas, T.; Daskeviciene, M.; Abate, A.; Ahmad, S.; Grätzel, M.; Getautis, V.; Nazeeruddin, M. K. A Methoxydiphenylamine-Substituted Carbazole Twin Derivative: An Efficient Hole-Transporting Material for Perovskite Solar Cells. *Angew. Chemie Int. Ed.* **2015**, *54* (39), 11409–11413.

(36) Wang, H.; Sheikh, A. D.; Feng, Q.; Li, F.; Chen, Y.; Yu, W.; Alarousu, E.; Ma, C.; Haque, M. A.; Shi, D.; Wang, Z.-S.; Mohammed, O. F.; Bakr, O. M.; Wu, T. Facile Synthesis and High Performance of a New Carbazole-Based Hole-Transporting Material for Hybrid Perovskite Solar Cells. *ACS Photonics* **2015**, *2* (7), 849–855.

(37) Zhang, X.; Zhou, Z.; Ma, S.; Wu, G.; Liu, X.; Mateen, M.; Ghadari, R.; Wu, Y.; Ding, Y.; Cai, M.; Dai, S. Fused Tetraphenylethylene–triphenylamine as an Efficient Hole Transporting Material in Perovskite Solar Cells. *Chem. Commun.* **2020**, *56* (21), 3159–3162.

(38) Zhu, Z.-L.; Chen, W.-C.; Zhang, L.-D.; Liu, X.-L.; Tong, Q.-X.; Wong, F.-L.; Lu, F.; Lee, C.-S. A Pyridine Based Meta-Linking Deep-Blue Emitter with High Conjugation Extent and Electroluminescence Efficiencies. *J. Mater. Chem. C* **2016**, *4* (26), 6249–6255.

(39) Qiu, J.; Liu, H.; Li, X.; Wang, S. Position Effect of Arylamine Branches on Pyrene-Based Dopant-Free Hole Transport Materials for Efficient and Stable Perovskite Solar Cells. *Chem. Eng. J.* **2020**, *387*, 123965.

(40) Liu, X.; Kong, F.; Ghadari, R.; Jin, S.; Chen, W.; Yu, T.; Hayat, T.; Alsaedi, A.; Guo, F.; Tan, Z.; Chen, J.; Dai, S. Thiophene–Arylamine Hole-Transporting Materials in Perovskite Solar Cells: Substitution Position Effect. *Energy Technol.* **2017**, *5* (10), 1788–1794.

(41) Wang, L.; Sheibani, E.; Guo, Y.; Zhang, W.; Li, Y.; Liu, P.; Xu, B.; Kloo, L.; Sun, L. Impact of Linking Topology on the Properties of Carbazole-Based Hole-Transport Materials and Their Application in Solid-State Mesoscopic Solar Cells. *Sol. RRL* **2019**, 1900196.

(42) Shi, Y.; Hou, K.; Wang, Y.; Wang, K.; Ren, H.; Pang, M.; Chen, F.; Zhang, S. Two Methoxyaniline-Substituted Dibenzofuran Derivatives as Hole-Transport Materials for Perovskite Solar Cells. *J. Mater. Chem. A* **2016**, *4* (15), 5415–5422.

(43) Li, D.; Shao, J. Y.; Li, Y.; Li, Y.; Deng, L. Y.; Zhong, Y. W.; Meng, Q. New Hole Transporting Materials for Planar Perovskite Solar Cells. *Chem. Commun.* **2018**, *54* (13), 1651–1654.

(44) Liu, X.; Kong, F.; Ghadari, R.; Jin, S.; Yu, T.; Chen, W.; Liu, G.; Tan, Z.; Chen, J.; Dai,

S. Anthracene–arylamine Hole Transporting Materials for Perovskite Solar Cells. *Chem. Commun.* **2017**, *53* (69), 9558–9561.

(45) Degbia, M.; Schmaltz, B.; Bouclé, J.; Grazulevicius, J. V.; Tran-Van, F. Carbazole Based Hole Transporting Materials for Solid State Dye Sensitizer Solar Cells: Role of the Methoxy Groups. *Polym. Int.* **2014**, *63* (8), 1387–1393.

(46) Liu, X.; Kong, F.; Guo, F.; Cheng, T.; Chen, W.; Yu, T.; Chen, J.; Tan, Z.; Dai, S. Influence of π-Linker on Triphenylamine-Based Hole Transporting Materials in Perovskite Solar Cells. *Dye. Pigment.* **2017**, *139*, 129–135.

(47) Jiang, Q.; Zhang, L.; Wang, H.; Yang, X.; Meng, J.; Liu, H.; Yin, Z.; Wu, J.; Zhang, X.; You, J. Enhanced Electron Extraction Using SnO_2 for High-Efficiency Planar-Structure $HC(NH_2)_2PbI_3$-Based Perovskite Solar Cells. *Nat. Energy* **2017**, *2* (1), 16177.

(48) Yu, W.; Yang, Q.; Zhang, J.; Tu, D.; Wang, X.; Liu, X.; Li, G.; Guo, X.; Li, C. Simple Is Best: A p-Phenylene Bridging Methoxydiphenylamine-Substituted Carbazole Hole Transporter for High-Performance Perovskite Solar Cells. *ACS Appl. Mater. Interfaces* **2019**, *11* (33), 30065–30071.

(49) Nakar, R.; Ramos, F. J.; Dalinot, C.; Marques, P. S.; Cabanetos, C.; Leriche, P.; Sanguinet, L.; Kobeissi, M.; Blanchard, P.; Faure-Vincent, J.; Tran-Van, F.; Berton, N.; Rousset, J.; Schmaltz, B. Cyclopentadithiophene and Fluorene Spiro-Core-Based Hole-Transporting Materials for Perovskite Solar Cells. *J. Phys. Chem. C* **2019**, *123* (37), 22767–22774.

(50) Qiu, J.; Liu, H.; Li, X.; Wang, S.; Zhang, F. Impact of 9-(4-methoxyphenyl) Carbazole and Benzodithiophene Cores on Performance and Stability for Perovskite Solar Cells Based on Dopant-Free Hole-Transporting Materials. *Sol. RRL* **2019**, *3* (10), 1900202.

(51) Bi, D.; Xu, B.; Gao, P.; Sun, L.; Grätzel, M.; Hagfeldt, A. Facile Synthesized Organic Hole Transporting Material for Perovskite Solar Cell with Efficiency of 19.8%. *Nano*

Energy **2016**, *23*, 138–144.

(52) Jeon, N. J.; Lee, H. G.; Kim, Y. C.; Seo, J.; Noh, J. H.; Lee, J.; Seok, S. Il. O-Methoxy Substituents in Spiro-OMeTAD for Efficient Inorganic-Organic Hybrid Perovskite Solar Cells. *J. Am. Chem. Soc.* **2014**, *136* (22), 7837–7840.

(53) Kim, H.-S.; Park, N.-G. Parameters Affecting I – V Hysteresis of $CH_3NH_3PbI_3$ Perovskite Solar Cells: Effects of Perovskite Crystal Size and Mesoporous TiO_2 Layer. *J. Phys. Chem. Lett.* **2014**, *5* (17), 2927–2934.

(54) Contreras-Bernal, L.; Salado, M.; Todinova, A.; Calio, L.; Ahmad, S.; Idígoras, J.; Anta, J. A. Origin and Whereabouts of Recombination in Perovskite Solar Cells. *J. Phys. Chem. C* **2017**, *121* (18), 9705–9713.

(55) Ebadi, F.; Taghavinia, N.; Mohammadpour, R.; Hagfeldt, A.; Tress, W. Origin of Apparent Light-Enhanced and Negative Capacitance in Perovskite Solar Cells. *Nat. Commun.* **2019**, *10* (1), 1574.

(56) Chi, D.; Huang, S.; Zhang, M.; Mu, S.; Zhao, Y.; Chen, Y.; You, J. Composition and Interface Engineering for Efficient and Thermally Stable Pb-Sn Mixed Low-Bandgap Perovskite Solar Cells. *Adv. Funct. Mater.* **2018**, *28* (51), 1804603.

(57) Chen, K.; Hu, Q.; Liu, T.; Zhao, L.; Luo, D.; Wu, J.; Zhang, Y.; Zhang, W.; Liu, F.; Russell, T. P.; Zhu, R.; Gong, Q. Charge-Carrier Balance for Highly Efficient Inverted Planar Heterojunction Perovskite Solar Cells. *Adv. Mater.* **2016**, *28* (48), 10718–10724.

(58) Cheng, H.; Li, Y.; Zhao, G.; Zhao, K.; Wang, Z.-S. Pyridine-Terminated Conjugated Organic Molecules as an Interfacial Hole Transfer Bridge for NiOx-Based Perovskite Solar Cells. *ACS Appl. Mater. Interfaces* **2019**, *11*, 28960–28967.

(59) Lv, X.; Xiao, G.; Feng, X.; Cao, J.; Yao, X.; Liu, J. Acylhydrazone-Based Porphyrin Derivative as Hole Transport Material for Efficient and Thermally Stable Perovskite Solar Cells. *Dye. Pigment.* **2019**, *160*, 957–961.

(60) Qiu, L.; He, S.; Ono, L. K.; Liu, S.; Qi, Y. Scalable Fabrication of Metal Halide Perovskite Solar Cells and Modules. *ACS Energy Lett.* **2019**, *4*, 2147–2167.

Table of Contents (TOC) graphic